PCCP

PAPER

View Article Online
View Journal

Cite this: DOI: 10.1039/c7cp07898f

Conflicting effect of chemical doping on the thermoelectric response of ordered PEDOT aggregates

Luigi Cigarini,[ab] Alice Ruini,[ab] Alessandra Catellani[b] and Arrigo Calzolari *[b]

Received 23rd November 2017,
Accepted 23rd January 2018

DOI: 10.1039/c7cp07898f

rsc.li/pccp

Poly(3,4-ethylenedioxythiophene) (PEDOT) semiconductor plays a relevant role in the development of organic thermoelectric (TE) devices for low-power generation. While dopant counterions are usually needed to provide electrical conductivity, their overall effects on the thermoelectric response of the systems are unknown and uncontrolled. Here, we present a first principles study of the electronic and thermal transport of PEDOT crystalline assemblies, specifically analysing the role played by tosylate dopants on the thermoelectric figure of merit of the doped system. Our results demonstrate that, beside the desired charging effect, the presence of dopants impacts the bulk configuration by inflating the packing structure and worsening the intrinsic transport properties of the PEDOT host. This provides a rationale for the necessity of controlling the optimal amount and the structural incorporation of dopant in order to maximize the thermoelectric response of organic materials.

1 Introduction

The perspective to apply thermoelectric conversion for power generators such as solar energy harvesting, wearable body heat conversion devices or coverage of industrial machines to recover waste energy fostered an increasing effort in research of organic thermoelectric (OTE) materials.[1] Flexibility, low cost, lightweight, easy chemical processability, and low optimal working temperatures are the major structural advantages of OTE with respect to inorganic thermoelectric (ITE) materials.[2–5] Still, the great limitation of OTEs is their current low efficiency in heat-to-electricity conversion, well below the standard values provided by inorganic systems but required for any realistic industrial application.[6] Thermoelectric conversion capability of materials is expressed by the dimensionless figure of merit: $zT = \sigma S^2 T/(k_{el} + k_{ph})$, where σ is the electrical conductivity of the material, S is the Seebeck coefficient, T is the absolute temperature, k_{el} and k_{ph} are, respectively, the electronic and phononic parts of the thermal conductivity.[6,7] OTE materials, which are generally composed of semi-conductive polymers, have intrinsically poor thermal transport properties and good Seebeck coefficients,[8,9] but their electrical conductivity is greatly lower than in ITE.[10] Among the plethora of polymeric compounds considered in experiments (*e.g.* polyanilines,[8,11–14] polypyrroles,[15] polycarbazoles,[16] polythiophenes[17]), PEDOT systems have gained particular attention for their stable processability and the large zT efficiency (compared to other OTEs).[18–22]

In general, in order to improve the TE response of a system, the main (often unique) effort is devoted to implement techniques (*e.g.* doping, chemical modifications, topological protection) able to increase its electron conductivity. This is also the case of OTEs for which both electrochemical[23,24] and chemical methods[25] are used to increase the electrical conductivity of pristine semiconducting host.[18,26] The concept is similar for the two approaches: the polymer chain is being oxidized by employing either external electrodes (electrochemical methods) or oxidizing agents (chemical method). Then, a dopant counterion (typically molecules or oligomers), coming from the solution or already present in the chemical oxidizing agent, stabilizes the positive charge on the polymer, restoring neutrality of the whole system.[27] The control and reproducibility of doping procedure is a major issue, as reproducibility largely depends on the environmental conditions and often results unsatisfactory. Electrochemical techniques generally guarantee better results in reproducibility, due to the accurate control of the imposed external potential but it is not suitable for samples thicker than 2 nm. Thus, oxidative techniques are nowadays the most used to produce doped polymeric blends. This approach generates conducting chains in their maximum oxidation state; successive dedoping procedures[9,11,13,17,20] are often exploited to tune the doping level.

In contrast with inorganic systems, where doping is generally obtained by including atomic aliovalent impurities that hardly affect the crystal structure, in the case of polymeric compounds

[a] Dipartimento FIM, Universitá di Modena e Reggio Emilia, I-41125, Modena, Italy
[b] CNR-NANO, Istituto Nanoscienze, Centro S3, via Campi 213A, I-41125, Modena, Italy. E-mail: arrigo.calzolari@nano.cnr.it; Fax: +39 059 367488; Tel: +39 059 2055627

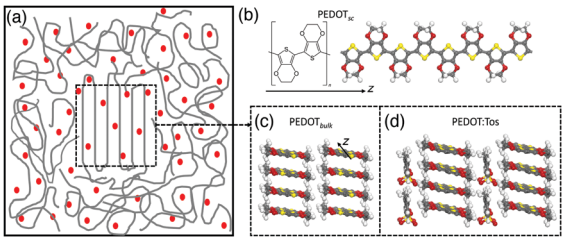

Fig. 1 (a) Pictorial representation of a disordered assembly of polymer (gray line) and counterions (red dots), which includes an ordered crystalline domain (dashed line). (b) Structure formula and atomic structure of periodic PEDOT single chain (PEDOT$_{sc}$). Crystal structure of (c) PEDOT$_{bulk}$ and (d) PEDOT:Tos. Polymer chains are aligned along z direction. The primitive cells in panel (b–d) are replicated along the three spatial directions for clarity.

doping affects the solid-state packing of the polymer assembly:[28,29] dopant counterions remain in the sample and inflate the bulk structure which alters the pristine inter-chain arrangement. These structural modifications are, to some extent, permanent and do not completely revert back with dedoping procedures. A typical consequence is an increase of spatial inhomogeneity and the creation of empty regions among polymer stacks, which influence both the electron and phonon transport in a way not easily predictable *a priori*.

In this regards, a first principles approach – able to simulate both electron and phonon carriers at the same level of accuracy – allows to gain insight on the microscopic effects of the structure and chemical composition on the TE of polymeric compounds. Although organic polymers are intrinsically disordered, the identification of locally ordered crystalline domains dispersed in the globally disordered matrix (Fig. 1a) has been widely documented and accepted in the literature.[9,30–33] In this work, we present a first principles investigation of TE characteristics of crystalline PEDOT phase, in the presence of tosylate (Tos) molecular counterion.[34] PEDOT:Tos system is known to display stability and high electrical conductivity[6,35] and can be routinely synthesized by different techniques, such as chemical and vapor phase polymerization.[9,36] We focus in particular on the effects that dopants have on thermal transport, which is usually ruled out from investigation of TE characteristics. The final aim is to gain insights on the (electron and phonon) transport mechanisms which take place in the local ordered domains, in consideration of the primary role they have in the general transport properties of the whole real systems. Our results indicate that, even though necessary to electron current flow, the presence of molecular dopants is detrimental for the TE response of the pristine PEDOT compound. This conflicting effect of dopants is highly unexplored and calls for a deeper understanding of the doping/dedoping processes to optimize the TE conversion capability of organic systems.

2 Method

Total-energy-and-forces optimization of the polymeric systems are carried out within the density functional theory (DFT) framework, as implemented in the Quantum Espresso[37] (QE) suite of codes. The exchange–correlation functional is described by using PBE[38] formulation of generalized gradient approximation and ultrasoft pseudopotentials[39] are used to treat the ionic potentials. Single particle Khon-Sham orbitals (charge densities) are expanded in plane waves up to a kinetic energy cutoff of 35.0 Ry (700.0 Ry), respectively. Grimme D2[40] correction are used to model the van der Waals type interactions. The convergence thresholds for the geometrical optimizations are set to 10^{-12} Ry for the total energy and 10^{-8} Ry per a.u. for the forces.

Extended systems are simulated by using periodically repeated supercells. The unit cell of the system (PEDOT$_{bulk}$) contains four EDOT monomers per cell, forming two parallel PEDOT chains, with two monomers per chain. PEDOT:Tos supercell contains four EDOT monomers (two parallel PEDOT chains) and a Tos dopant unit. This corresponds to a 1 : 4 doping ratio, close to the maximum doping concentration that can be obtained experimentally. The initial atomic positions have been borrowed from X-ray diffraction measurements.[24] Charge neutrality of PEDOT:Tos is assured by removing a hydrogen atom from a *p*-toluenesulfonic unit. The charge separation between the negative tosylate ion and the positive PEDOT chains is not imposed *a priori*, but rather results from the DFT calculation. Single polymer chain (PEDOT$_{sc}$), considered for comparison, is simulated setting the two repeated monomers in a cell surrounded by a thick layer of vacuum in the directions perpendicular to the polymer axis, so to let interpolymer interactions vanish. Summations over the crystal Brillouin zones are done using uniform Monkorst–Pack grids of $(3 \times 4 \times 4)$, $(8 \times 8 \times 8)$ and $(1 \times 1 \times 8)$ k-points for PEDOT:Tos, PEDOT$_{bulk}$ and PEDOT$_{sc}$, respectively. In all cases polymer chains are aligned along the z axis (Fig. 1).

Coherent transport properties (*i.e.* electron $\mathcal{T}_{el}(E)$ and phonon $\mathcal{T}_{ph}(E)$ quantum transmittance) are calculated from first principles by using the WanT code,[41,42] which implements the Landauer formula for both fermion and boson carriers within a real-space Green's function framework.[43] In particular, real-space Hamiltonian matrices are evaluated through a recent-developed projection-filtering technique,[44,45] which allows to map the original Hamiltonians resulting from DFT calculations and expressed in plane waves into tight-binding (TB) matrices operating into a much smaller space spanned by a set of atomic orbitals. This procedure combines the accuracy and the predictive value of first-principles approaches with the low computational cost of TB techniques. The phonon counterpart is simulated starting from the *ab initio* calculation of the interatomic force matrices,[46] obtained with a finite-differences/finite-fields approach,[47] that has been demonstrated to be computationally very efficient in the simulation of the vibrational spectra of both inorganic[47] and molecular crystals.[48]

All the ingredients entering in the zT expression can be easily derived from electron and phonon transmittances, by using the intermediate kinetic functions $L_n(\mu,T)$ (see *e.g.* ref. 49). Notably, in the coherent transport approximation, the figure of merit reduces to $zT = S^2 G_{el} T/K_t$,[50] where G_{el} and $K_t = K_{el} + K_{ph}$ are the corresponding quantum conductance terms. For further details on the

accuracy and capability of the present approach we refer to previous works.[46,48,51,52]

3 Results and discussion

In order to decouple the solid-state and doping effects, we studied the PEDOT bulk crystal with and without the tosylate dopant. Single PEDOT chain is also considered for comparison. Along the chain, PEDOT presents a $\sim 180^\circ$ alternating rotation angle between adjacent monomers (Fig. 1b). In the crystalline phases, the aromatic planes of adjacent chains are parallel and vertically stacked, and longitudinally shifted one respect to the other for the length of one monomer (Fig. 1c and d). The optimized cell parameters for the $PEDOT_{bulk}$ are a = 10.52 Å, b = 7.10 Å, c = 7.81 Å, being z the direction of the chains and y the direction perpendicular to the aromatic planes (*i.e.* the stacking direction). The cell parameters after the inclusion of Tos unit change to a = 13.67 Å, b = 6.78 Å, c = 7.78 Å. In both cases, the periodic pitches (c) of the polymers in the bulk phase are slightly different from the single chain one (c = 7.87 Å). This means that inter-chain (vertical and lateral) packing from one side and spatial hindrance of the dopant on the other side impart a progressive reduction of the periodicity of the polymer (*i.e.* intra-chain compression), which results in the modification of electronic conjugation and phonon stiffness of PEDOT systems, and thus of their TE properties, as we discuss in the following.

In Fig. 2 we report the zT functions for $PEDOT_{bulk}$ and PEDOT:Tos systems, calculated at room temperature (300 K) and as a function of the electron chemical potential. The two functions have been aligned to the valence band maximum of the two electronic band structures, while the zero energy reference has been set at the Fermi level of the clean $PEDOT_{bulk}$ structure. Being interested in p-type doping, we focus on negative values of the electron chemical potential. As expected, the two PEDOT systems (with and without dopant) exhibit an overall similarity: most of the peaks in the zT plots are common for both structures and have similar energies. However, the intensity of the peaks and the actual position of the Fermi level remark the differences induced by the Tos dopant. Except for the unique peak at $\simeq -3$ eV, the zT absolute values of PEDOT:Tos are systematically lower with respect to $PEDOT_{bulk}$, which leads to the conclusion that the presence of doping, albeit necessary to have electrical conduction, is detrimental to the intrinsic TE properties of PEDOT. We further note that in both cases the maximum value of zT at -0.3 eV does not match the Fermi level of the system. In particular, for PEDOT:Tos at the chemical potential corresponding to the Fermi level (red vertical line) zT is almost zero, despite the electron transport is ensured by doping. This observation is also in agreement with the low experimental values measured for PEDOT crystals. This drives us to two conclusions: (i) Tos chemical doping does not optimize the TE characteristics of PEDOT; (ii) improving electron transport is a necessary but not sufficient condition for an efficient thermoelectric response.

In order to unravel the microscopic origins of these features, we analyze the electronic and thermal contributions to zT figure of merit of PEDOT. The electronic properties for the studied systems are displayed in Fig. 3, where we compare the results of the single chain $PEDOT_{sc}$ (panel a) with $PEDOT_{bulk}$ (panel b) and PEDOT:Tos (panel c). For each system, Fig. 3 shows the calculated band structures (middle) together with the correspondent Seebeck coefficient (left) and electronic transmission function (right). To help comparison and to be consistent with the results in Fig. 2, the zero value of the scale has been set at the Fermi level of the clean $PEDOT_{bulk}$ structure. The electronic properties of the isolated chain have been largely discussed in a previous work.[48] Here we report a few data to elucidate the effects induced by the solid state packing. $PEDOT_{sc}$ is a semiconducting system characterized by two main dispersive bands along the chain direction (Γ–Z) separated by a direct Khon–Sham bandgap of 0.92 eV at Γ. Moving from single chain to 3D bulk (Fig. 3b) entails a remarkable modification in the bandstructure. Although the system remains semiconducting, the structural distortions described above along with π–π and van der Waals interchain coupling affect both the shape and the degeneracy of the bands close to the Fermi level for all

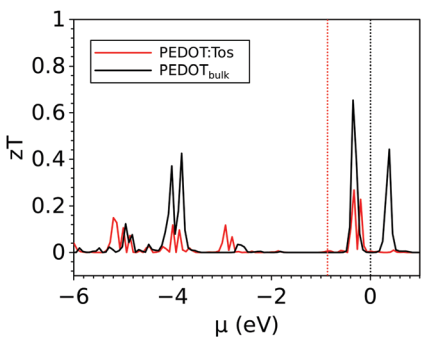

Fig. 2 The calculated zT values as a function of the electron chemical potential (μ) for T = 300 K. The valence bands have been aligned, and the energy zero is set to the Fermi level of the $PEDOT_{bulk}$. Vertical dotted lines correspond to the Fermi energy of the two systems.

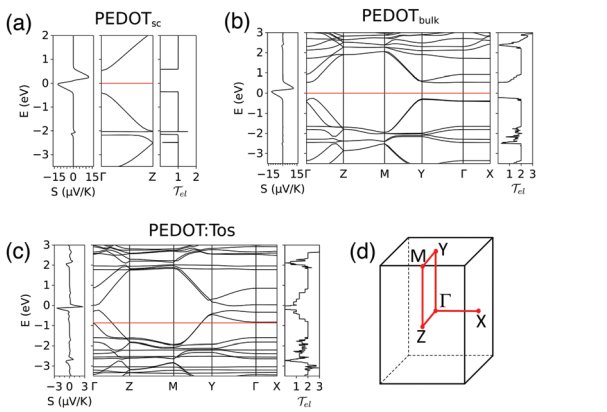

Fig. 3 Electronic properties of (a) $PEDOT_{sc}$, (b) $PEDOT_{bulk}$, (c) PEDOT:Tos. Each panel includes (left) Seebeck coefficient S; (middle) the bandstructure, and (right) the electronic transmission function $\mathscr{T}_{el}$ in unit of $2e^2/h$. Horizontal red lines mark the Fermi level of each system. Band alignment and zero energy reference follow Fig. 2. (d) Orthorhombic Brillouin zone and high symmetry points corresponding to bandstructures of panels (a–c).

spatial directions. Interchain interactions induce band splitting along the polymer chain direction and variation of the *k*-dispersion for the highest occupied and lowest unoccupied bands, which reduce (0.77 eV) and shift the bandgap from the center of BZ along the Γ–Z line. In the directions perpendicular to aromatic planes (Y–Γ) the π–π interaction is responsible for a sub-band splitting, especially of conduction bands, while inter-chain lateral coupling (Γ–X direction) does not induce any relevant band dispersion. The resulting bandstructures for $PEDOT_{sc}$ and $PEDOT_{bulk}$ perfectly reproduce previous theoretical results.[53,54] When both crystal-field and doping effects are included (Fig. 3c), we observe further changes in the electronic structure of the system that now acts as a degenerate p-type conductor, with the Fermi level which lies deep inside the valence band of the pristine PEDOT bulk ($\simeq -1$ eV). The lateral presence of Tos unit affects the stacking of PEDOT chains, reducing the pristine gap of the bulk to 0.22 eV and increasing the band splitting along the Γ–X direction. Moreover, a new set of flat occupied bands clearly appear in the PEDOT:Tos bandstructure, which stem from the localized orbitals of the tosylate ions. The presence of these dopant-related states and the changes in the shape of the electronic bands rule out a mere rigid-band description for the doped system over a wide energy range, as used in implicit doping models.

The lateral panels of Fig. 3 present respectively the Seebeck (left) and the electronic transmission (right) functions for the PEDOT systems. Transmission functions have the expected step-like feature typical of periodic systems, with a direct correspondence between the number of quanta of conductance and the number of bands available for conduction at each energy level. The quantum conductance $G_{el} = \mathscr{T}_{el}(E_F)$ that enters in the zT figure of merit is zero for $PEDOT_{sc}$ and $PEDOT_{bulk}$, and is equal to $2\mathscr{G}_0$ for PEDOT:Tos, where $\mathscr{G}_0 = 2e^2/h$ is the quantum of electron conductance. The Seebeck coefficient of undoped $PEDOT_{bulk}$ presents close similarities with that of single chain, in correspondence of the band gap. On the contrary the Seebeck coefficient for PEDOT:Tos is scaled by $\sim 1/5$ with respect to $PEDOT_{bulk}$. This follows the general rule that correlates the S, σ_{el}, and κ_{el}: increasing the σ_{el} generally results in decreasing of both S[55] and κ_{el} (Wiedemann–Franz law).

In contrast to electronic parameters that enter in the figure of merit, the phononic part is independent from the chemical potential, thus it can not be controlled *via* an implicit doping model, but requires the explicit description of dopant counterions. Fig. 4 shows the calculated phononic thermal conductances κ_{ph} as a function of temperature for the three considered systems. For each temperature, we observe a progressive reduction of κ_{ph} moving from PEDOT:Tos, to $PEDOT_{bulk}$ and $PEDOT_{sc}$, respectively. In particular, solid-state effects impart smaller changes in the κ_{ph} spectrum than doping.

The analysis of the phonon bands (Fig. 5) highlights the most active modes in heat transport along the chains, *i.e.* the ones that contribute to the TE process. The main contributions come from the q-dispersive modes along the Γ–Z direction in an energy range between 0 and 600 cm^{-1}. For the two bulk systems, *e.g.*, this spectral region is responsible for $\sim$85% of

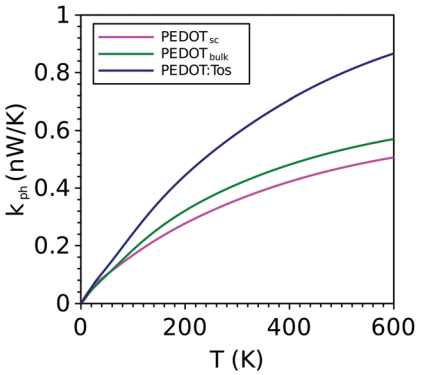

Fig. 4 Lattice thermal conductance of $PEDOT_{sc}$, $PEDOT_{bulk}$ and PEDOT:Tos simulated systems, reported as a function of the temperature.

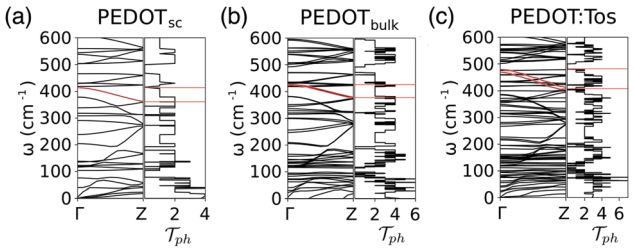

Fig. 5 Phononic (left) bandstructures and (right) total transmission function of the (a) $PEDOT_{sc}$, (b) $PEDOT_{bulk}$ and (c) PEDOT:Tos. Only the lower frequency portion of the spectrum, up to 600 cm^{-1}, is reported. Horizontal red lines mark the regions which mostly affect the corresponding κ_{ph} of Fig. 4.

the lattice thermal conduction, at 300 K (Fig. 4). The analysis of the frequency regions that most contribute to the thermal conductance reveals the primary role of acoustic bands at low frequency as well as of a dispersive band at higher frequencies (red line in Fig. 5). The latter is associated to an in-phase out-of-plane displacement of carbon atoms, which propagates along the polymer backbone (Fig. 6). Even though homologous modes can be recognized in all the three systems, the details and the intensity of the modes actually depend on the specific structural arrangement. Thus, with respect to $PEDOT_{sc}$, van der Waals and π–π interactions break the chain equivalence in the bulk crystal. This gives rise to a splitting of the acoustic branches in $PEDOT_{bulk}$ and a slight blue shift of the lowest optical modes: this is an indication that the presence of lateral chains, though not chemically bonded, constrain the vibrational degrees of freedom of the single chain, making the system more stiff. Notably, this symmetry breaking imparts a reduction of the transmittance per chain, in agreement with previous theoretical and experimental results on similar polymeric systems.[56,57] However, since the phonon transport is an integrated quantity, the sum over all chains in the bulk assemblies gives rise to an overall increase of $\mathscr{T}_{ph}$ and thus of κ_{ph}.

A close comparison with available experimental data shows that our calculated zT are of the same order of magnitude of the optimal measured values (that for PEDOT:Tos systems is around 0.25[20]). It is also meaningful to discuss the role of all

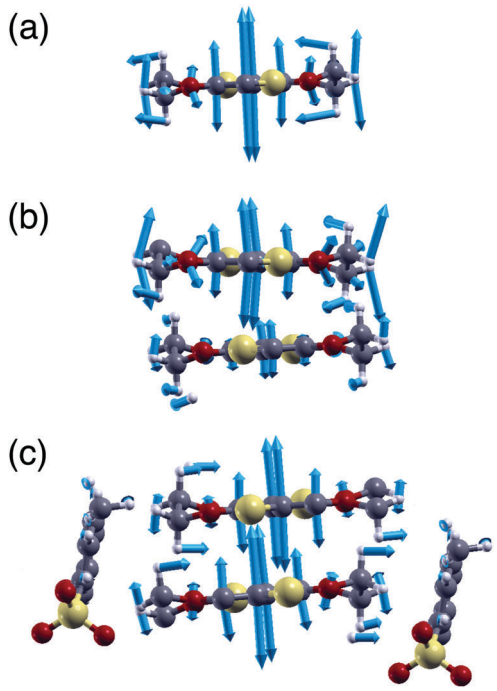

Fig. 6 Side view of atomic displacement of selected phonon modes at for (a) $PEDOT_{sc}$ at 413 cm^{-1}, (b) $PEDOT_{bulk}$ at 425 cm^{-1}, and (c) PEDOT:Tos at 460 cm^{-1}.

the parameters entering the figure of merit, namely the electrical conductivity, the Seebeck coefficient and the thermal conductivity, along with their comparison to experiments. The electric conductance values calculated here refer to ideal, perfectly ordered systems, and therefore surely overestimate the electronic transport efficiency of the real systems; a direct comparison between numerical values however cannot be obtained due to the difference between the two physical quantities (calculated conductance and measured conductivity). The calculated value for the Seebeck coefficient reaches its maximum for the case of the $PEDOT_{bulk}$ system (S = 11.2 μV K^{-1}), and it underestimates the typical experimental values (S = 40 μV K^{-1} at an oxidation level of 36%[20]). For what concerns the thermal conductivity, our calculated value for the lattice contribution (0.386 W $(m\ K)^{-1}$) is in very good agreement with the experimentally reported thermal conductivities (*e.g.* 0.37 W $(m\ K)^{-1}$ with an error bar of 10% for PEDOT-Tos[20]); this satisfactory comparison also suggests that the detrimental effect due to electron–phonon interaction recently observed for some bulk metals[58] and heavily-doped semiconductors[59] should not be crucial for the here investigated systems.

Our calculations show that the inclusion of dopants sums up to solid-state effects and it is responsible for the appearance of undispersive (molecular-like) vibrational modes in the phonon bandstructure. Even though Tos does not directly participate to the coherent thermal transport along the chain it has an overall indirect effect, as it changes the lateral packing of PEDOT. This effect is hard to quantify but it can be envisaged, *e.g.*, focusing on the red-dispersive band discussed above that results blue shifted and more dispersive. The presence of lateral Tos units reduces the overall PEDOT density, but it seems to preserve the character of the pristine target red band. The corresponding mode (Fig. 6c) close resembles the single chain case, with an almost normal displacement of the carbon atoms, with respect to the polymer plane. Rather the tight lateral inter-chain packing in $PEDOT_{bulk}$ (Fig. 6b), introduces tangential components that do not contribute to transport. Thus, the apparently low enhancement of vibrational mode density in the range 400–500 cm^{-1} is the main responsible of the net enhancement in the thermal conductance of PEDOT:Tos with respect to the undoped bulk.

We can conclude that the inclusion of Tos dopant increases the overall degrees of freedom for phonon transport which results in a subtle enhancement of the thermal conductance and thus in a reduction of the corresponding zT. It worth noticing that: (i) our simulated PEDOT:Tos system represents an highly doped system (doping ratio 1 : 4). Different doping levels may alter the polymer density/packing and thus the effects on the thermal transport. Considering also the electronic effects, the research of an optimal doping level is necessary to maximize the thermoelectric performances. This includes also the necessity of controlling the dedoping procedures, which remove the presence of excess counterions, leaving empty spaces in the bulk structure of the polymers.[60] (ii) The inclusion of polymeric dopants (*e.g.* PSS) instead of molecular ones may further increase the phonon transport along the dopant chains, with a negative effect for the TE conversion. (iii) The persistence of a phonon density of states in the THz and mid-IR range has seeded new paradigms in hybrid TE-organic/TE-inorganic nanostructures (such as Bi_2Te_3 wires embedded in PEDOT:PSS matrices[61]) that are expected to benefit of the best characteristics of the two separate components: the low thermal conductivity of polymeric systems and the high electron conductivity of inorganic wires. The idea is based on the so-called energy filtering effect[62–64] that exploits the phonon energy superpositions of the two materials to convey the thermal transport into the polymeric blend so to reduce the lattice conductivity in the inorganic counterpart, giving a higher overall TE efficiency.

4 Conclusions

We present a fully first principles investigation of the effect of tosylate dopants on the thermoelectric properties of crystalline PEDOT assemblies, which have an important relevance also for disordered systems. The explicit treatment of both electronic and vibrational degrees of freedom, at the same level of accuracy, allowed us to gain insights on the consequences of solid-state effects and doping at the atomistic level. Our results demonstrate that, albeit necessary to impart electron conductivity to the polymeric system (positive effect), the inclusion of Tos has also detrimental effects on both electronic and thermal conductivity of PEDOT bulk. In particular, the presence of the Tos unit entails two main effects: (i) it dopes the PEDOT bulk by pinning the Fermi level into the valence band of the host, (ii) it changes the spatial assembly of the PEDOT chains, with a consequent change in the electronic and vibrational properties.

At the specific doping ratio considered in this work, the resulting position of the Fermi level does not fit the maximum possible values for *zT* at room temperature. Further, even though Tos does not directly contribute to the coherent thermal transport, it has an indirect enhancement effect on the phonon conductance of the polymer, which worsen the TE response of the system. While the effect of doping on the electronic properties may be described to some extents within an implicit doping model, the effects of the thermal transport requires the explicit (atomistic) treatment of the dopant impurities. The *zT* peak values calculated here can be considered an upper-limit estimate of the *zT* figure of merit, in qualitative agreement with most experimental results. Indeed, although the electric conductance values calculated here overestimate the average experimental values of conductivity (caused by neglecting the dissipation scattering effects of the present approach), the Seebeck coefficient and thermal conductance values are in the same order of magnitude of the corresponding experimental ones.

Conflicts of interest

There are no conflicts to declare.

Acknowledgements

We acknowledge the CINECA award under the ISCRA initiative, for the availability of high performance computing resources and support.

References

1 A. R. M. Siddique, S. Mahmud and B. Van Heyst, *Renewable Sustainable Energy Rev.*, 2017, **73**, 730–744.
2 B. Russ, A. Glaudell, J. J. Urban, M. L. Chabinyc and R. A. Segalman, *Nat. Rev. Mater.*, 2016, **1**, 16050.
3 Q. Zhang, Y. Sun, W. Xu and D. Zhu, *Adv. Mater.*, 2014, **26**, 6829–6851.
4 J. J. Lee, D. Yoo, C. Park, H. H. Choi and J. H. Kim, *Sol. Energy*, 2016, **134**, 479–483.
5 O. Bubnova and X. Crispin, *Energy Environ. Sci.*, 2012, **5**, 9345–9362.
6 M. H. Elsheikh, D. A. Shnawah, M. F. M. Sabri, S. B. M. Said, M. H. Hassan, M. B. A. Bashir and M. Mohamad, *Renewable Sustainable Energy Rev.*, 2014, **30**, 337–355.
7 H. J. Goldsmid, *Introduction to Thermoelectricity*, Springer, Berlin, Heidelberg, 2016.
8 H. Yan, N. Sada and N. Toshima, *J. Therm. Anal. Calorim.*, 2002, **69**, 881–887.
9 O. Bubnova, Z. U. Khan, H. Wang, S. Braun, D. R. Evans, M. Fabretto, P. Hojati-Talemi, D. Dagnelund, J.-B. Arlin, Y. H. Geerts, S. Desbief, D. W. Breiby, J. W. Andreasen, R. Lazzaroni, W. M. Chen, I. Zozoulenko, M. Fahlman, P. J. Murphy, M. Berggren and X. Crispin, *Nat. Mater.*, 2014, **13**, 190–194.
10 Y. Du, S. Z. Shen, K. Cai and P. S. Casey, *Prog. Polym. Sci.*, 2012, **37**, 820–841.
11 J. Li, X. Tang, H. Li, Y. Yan and Q. Zhang, *Synth. Met.*, 2010, **160**, 1153–1158.
12 Y. Sun, Z. Wei, W. Xu and D. Zhu, *Synth. Met.*, 2010, **160**, 2371–2376.
13 J. Jin, Q. Wang and M. A. Haque, *J. Phys. D: Appl. Phys.*, 2010, **43**, 205302.
14 C. Cho, B. Stevens, J.-H. Hsu, R. Bureau, D. A. Hagen, O. Regev, C. Yu and J. C. Grunlan, *Adv. Mater.*, 2015, **27**, 2996–3001.
15 Z. Zhang, G. Chen, H. Wang and W. Zhai, *J. Mater. Chem. C*, 2015, **3**, 1649–1654.
16 I. Levesque, P.-O. Bertrand, N. Blouin, M. Leclerc, S. Zecchin, G. Zotti, C. I. Ratcliffe, D. D. Klug, X. Gao, F. Gao and J. S. Tse, *Chem. Mater.*, 2007, **19**, 2128–2138.
17 B. Endroï£¡di, J. Mellar, Z. Gingl, C. Visy and C. Janaky, *J. Phys. Chem. C*, 2015, **119**, 8472–8479.
18 G.-H. Kim, L. Shao, K. Zhang and K. P. Pipe, *Nat. Mater.*, 2013, **12**, 719–723.
19 R. Yue and J. Xu, *Synth. Met.*, 2012, **162**, 912–917.
20 O. Bubnova, Z. U. Khan, A. Malti, S. Braun, M. Fahlman, M. Berggren and X. Crispin, *Nat. Mater.*, 2011, **10**, 429–433.
21 D. Yoo, J. Kim, S. H. Lee, W. Cho, H. H. Choi, F. S. Kim and J. H. Kim, *J. Mater. Chem. A*, 2015, **3**, 6526–6533.
22 B. Zhang, J. Sun, H. E. Katz, F. Fang and R. L. Opila, *ACS Appl. Mater. Interfaces*, 2010, **2**, 3170–3178.
23 L. Zhang, T. Goto, I. Imae, Y. Sakurai and Y. Harima, *J. Polym. Sci., Part B: Polym. Phys.*, 2017, **55**, 524–531.
24 K. Aasmundtveit, E. Samuelsen, O. Inganäs, L. Pettersson, T. Johansson and S. Ferrer, *Synth. Met.*, 2000, **113**, 93–97.
25 M. N. Gueye, A. Carella, N. Massonnet, E. Yvenou, S. Brenet, J. Faure-Vincent, S. Pouget, F. Rieutord, H. Okuno, A. Benayad, R. Demadrille and J.-P. Simonato, *Chem. Mater.*, 2016, **28**, 3462–3468.
26 C. K. Chiang, C. R. Fincher, Y. W. Park, A. J. Heeger, H. Shirakawa, E. J. Louis, S. C. Gau and A. G. MacDiarmid, *Phys. Rev. Lett.*, 1977, **39**, 1098–1101.
27 P. Chandrasekhar, *Conducting polymers, fundamentals and applications: a practical approach*, Springer Science & Business Media, 2013.
28 A. M. Glaudell, J. E. Cochran, S. N. Patel and M. L. Chabinyc, *Adv. Energy Mater.*, 2015, **5**, 1401072.
29 M. Culebras, C. Gómez and A. Cantarero, *Materials*, 2014, **7**, 6701–6732.
30 D. C. Martin, J. Wu, C. M. Shaw, Z. King, S. A. Spanninga, S. Richardson-Burns, J. Hendricks and J. Yang, *Polym. Rev.*, 2010, **50**, 340–384.
31 A. G. MacDiarmid, *Synth. Met.*, 2001, **40**, 2581–2590.
32 A. Ferretti, A. Ruini, E. Molinari and M. J. Caldas, *Phys. Rev. Lett.*, 2003, **90**, 086401.
33 A. Ferretti, A. Ruini, G. Bussi, E. Molinari and M. J. Caldas, *Phys. Rev. B: Condens. Matter Mater. Phys.*, 2004, **69**, 205205.
34 K. Wijeratne, M. Vagin, R. Brooke and X. Crispin, *J. Mater. Chem. A*, 2017, **5**, 19619–19625.
35 Z. U. Khan, O. Bubnova, M. J. Jafari, R. Brooke, X. Liu, R. Gabrielsson, T. Ederth, D. R. Evans, J. W. Andreasen,

M. Fahlman and X. Crispin, *J. Mater. Chem. C*, 2015, **3**, 10616–10623.
36 L. H. Jimison, A. Hama, X. Strakosas, V. Armel, D. Khodagholy, E. Ismailova, G. G. Malliaras, B. Winther-Jensen and R. M. Owens, *J. Mater. Chem.*, 2012, **22**, 19498–19505.
37 P. Giannozzi, S. Baroni, N. Bonini, M. Calandra, R. Car, C. Cavazzoni, D. Ceresoli, G. Chiarotti, M. Cococcioni, I. Dabo, A. Dal Corso, S. De Gironcoli, S. Fabris, G. Fratesi, R. Gebauer, U. Gerstmann, C. Gougoussis, A. Kokalj, M. Lazzeri, L. Martin-Samos, N. Marzari, F. Mauri, R. Mazzarello, S. Paolini, A. Pasquarello, L. Paulatto, C. Sbraccia, S. Scandolo, G. Sclauzero, A. P. Seitsonen, A. Smogunov, P. Umari and R. M. Wentzcovitch, *J. Phys.: Condens. Matter*, 2009, **21**, 395502.
38 J. P. Perdew, K. Burke and M. Ernzerhof, *Phys. Rev. Lett.*, 1996, **77**, 3865–3868.
39 D. Vanderbilt, *Phys. Rev. B: Condens. Matter Mater. Phys.*, 1990, **41**, R7892–R7895.
40 S. Grimme, *J. Comput. Chem.*, 2006, **27**, 1787–1799.
41 A. Calzolari, N. Marzari, I. Souza and M. Buongiorno Nardelli, *Phys. Rev. B: Condens. Matter Mater. Phys.*, 2004, **69**, 035108.
42 WANT code by A. Ferretti, L. Agapito, A. Calzolari, and M. Buongiorno Nardelli, www.wannier-transport.org.
43 M. Buongiorno Nardelli, *Phys. Rev. B: Condens. Matter Mater. Phys.*, 1999, **60**, 7828–7833.
44 L. A. Agapito, A. Ferretti, A. Calzolari, S. Curtarolo and M. Buongiorno Nardelli, *Phys. Rev. B: Condens. Matter Mater. Phys.*, 2013, **88**, 165127.
45 P. D'Amico, L. Agapito, A. Catellani, A. Ruini, S. Curtarolo, M. Fornari, M. Buongiorno Nardelli and A. Calzolari, *Phys. Rev. B*, 2016, **94**, 165166.
46 A. Calzolari, T. Jayasekera, K. W. Kim and M. Buongiorno Nardelli, *J. Phys.: Condens. Matter*, 2012, **24**, 492204.
47 A. Calzolari and M. Buongiorno Nardelli, *Sci. Rep.*, 2013, **3**, 2999.
48 L. Cigarini, A. Ruini, A. Catellani and A. Calzolari, *J. Phys. D: Appl. Phys.*, 2017, **50**, 395502.
49 G. Grosso and G. Pastori Parravicini, *Solid State Physics*, Academic Press Elsevier Ltd, Amsterdam NL, 2nd edn, 2014.
50 Y. Ouyang and J. Guo, *Appl. Phys. Lett.*, 2009, **94**, 263107.
51 Y. Chen, T. Jayasekera, A. Calzolari, K. W. Kim and M. Buongiorno Nardelli, *J. Phys.: Condens. Matter*, 2010, **22**, 372202.
52 A. Catellani, A. Ruini, M. B. Nardelli and A. Calzolari, *RSC Adv.*, 2015, **5**, 44865–44872.
53 W. Shi, T. Zhao, J. Xi, D. Wang and Z. Shuai, *J. Am. Chem. Soc.*, 2015, **137**, 12929–12938.
54 E.-G. Kim and J.-L. Brédas, *J. Am. Chem. Soc.*, 2008, **130**, 16880–16889.
55 N. Mateeva, H. Niculescu, J. Schlenoff and L. R. Testardi, *J. Appl. Phys.*, 1998, **83**, 3111–3117.
56 A. Henry, G. Chen, S. J. Plimpton and A. Thompson, *Phys. Rev. B: Condens. Matter Mater. Phys.*, 2010, **82**, 144308.
57 S. F. Parker, *J. Chem. Soc., Faraday Trans.*, 1996, **92**, 1941–1946.
58 Y. Wang, Z. Lu and X. Ruana, *J. Appl. Phys.*, 2016, **119**, 225109.
59 B. Liao, B. Qiu, J. Zhou, S. Huberman, K. Esfarjani and G. Chen, *Phys. Rev. Lett.*, 2015, **114**, 115901.
60 H. Park, S. H. Lee, F. S. Kim, H. H. Choi, I. W. Cheong and J. H. Kim, *J. Mater. Chem. A*, 2014, **2**, 6532–6539.
61 X. Tang, W. Xie, H. Li, W. Zhao, Q. Zhang and M. Niino, *Appl. Phys. Lett.*, 2007, **90**, 012102.
62 D. Narducci, E. Selezneva, G. Cerofolini, S. Frabboni and G. Ottaviani, *J. Solid State Chem.*, 2012, **193**, 19–25.
63 Z. Liang, M. J. Boland, K. Butrouna, D. R. Strachan and K. R. Graham, *J. Mater. Chem. A*, 2017, **5**, 15891–15900.
64 T. H. Zou, X. Y. Qin, D. Li, G. L. Sun, Y. C. Dou, Q.-Q. Wang, B. J. Ren, J. Zhang, H. X. Xin and Y. Y. Li, *Appl. Phys. Lett.*, 2014, **104**, 013904.